# Supplementary Material for

# Discovery of evidence of the Chicxulub impact in East Asia

Hayu Ota[1], Junichiro Kuroda[2], Keiichi Hayashi[3], Hiroyuki Hoshi[4], Ken Sawada[5], Hiroshi Nishi[6], Akira Ishikawa[7], and Reishi Takashima[8]

[1] Atmosphere and Ocean Research Institute, The University of Tokyo, Kashiwa, Chiba, Japan (h-ota@g.ecc.u-tokyo.ac.jp)

[2] Atmosphere and Ocean Research Institute, The University of Tokyo, Kashiwa, Chiba, Japan (kuroda@aori.u-tokyo.ac.jp)

[3] Research Institute of Energy, Environmental and Geology, Hokkaido Research Organization, Sapporo, Hokkaido, Japan (hayashi-keiichi@hro.or.jp)

[4] Aichi University of Education, Kariya, Aichi, Japan (hoshi@auecc.aichi-edu.ac.jp)

[5] Hokkaido University, Sapporo, Hokkaido, Japan (sawadak@sci.hokudai.ac.jp)

[6] Dinosaurs Research Institute, Fukui Prefectural University, Yoshida-gun Eiheijicho, Fukui, Japan (hnishi@tohoku.ac.jp)

[7] Institute of Science Tokyo, Meguro-ku, Tokyo, Japan (akr@eps.sci.titech.ac.jp)

[8] The Center for Academic Resources and Archives, Tohoku University Museum, Sendai, Miyagi, Japan (reishi.takashima.a7@tohoku.ac.jp)

# Contents

## 1. Osmium isotope system

Osmium (Os) is one of PGEs and has seven stable nuclides with mass numbers of 184, 186, 187, 188, 189, 190 and 192. Of these, $^{187}Os$ is the daughter nuclide of $^{187}Re$, which has a half decay period of 41.6 billion years (Smoliar et al., 1996). Rhenium (Re) is more easily concentrated in the liquid phase during the differentiation of the Earth than is Os, therefore Re/Os in the upper continental crust is higher than in meteorite and mantle. A high Re/Os ratio means a high radiogenic parent/daughter ratio, so the continental crust has a high $^{187}Os/^{188}Os$ ratio as time passed since the rocks were formed (Figure S1A). Marine Os isotope ratio ($^{187}Os/^{188}Os$) reflects the balance between Os flux from upper continental crust ($^{187}Os/^{188}Os$ ≈1.0-1.5), mantle ($^{187}Os/^{188}Os$ ≈0.12) and extraterrestrial material ($^{187}Os/^{188}Os$ ≈0.12) (Figure S1B). Secular variations in paleo-seawater $^{187}Os/^{188}Os$ ratio at that time are preserved in seafloor sediments. In addition, direct analysis of seawater $^{187}Os/^{188}Os$ ratios and Os concentrations around the world have confirmed that they are nearly homogeneous (e.g. Sharma et al., 2019). The marine Os residence time has been estimated to be 10,000 to 40,000 years (Peucker-Ehrenbrink & Ravizza, 2000, Lee et al., 2003), which is longer than the period of the ocean circulation.

The low abundance and short residence time of Os in the ocean mean that marine $^{187}Os/^{188}Os$ values could sharply respond to an instantaneous event, such as asteroid impact (Paquay et al., 2008, Sato et al., 2013). Declines in $^{187}Os/^{188}Os$ ratio also occur when large amounts of unradiogenic Os are supplied to seawater due to increased hydrothermal fluxes and weathering of young igneous rocks associated with large-scale igneous activity.

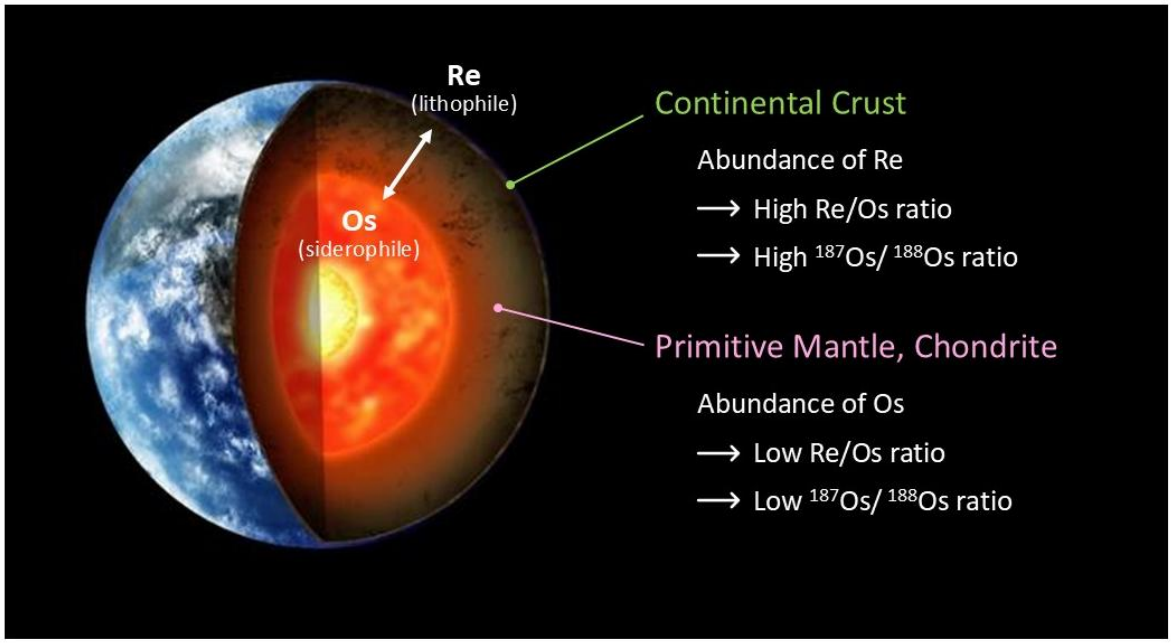


Figure S1A. The marine Osmium isotope system

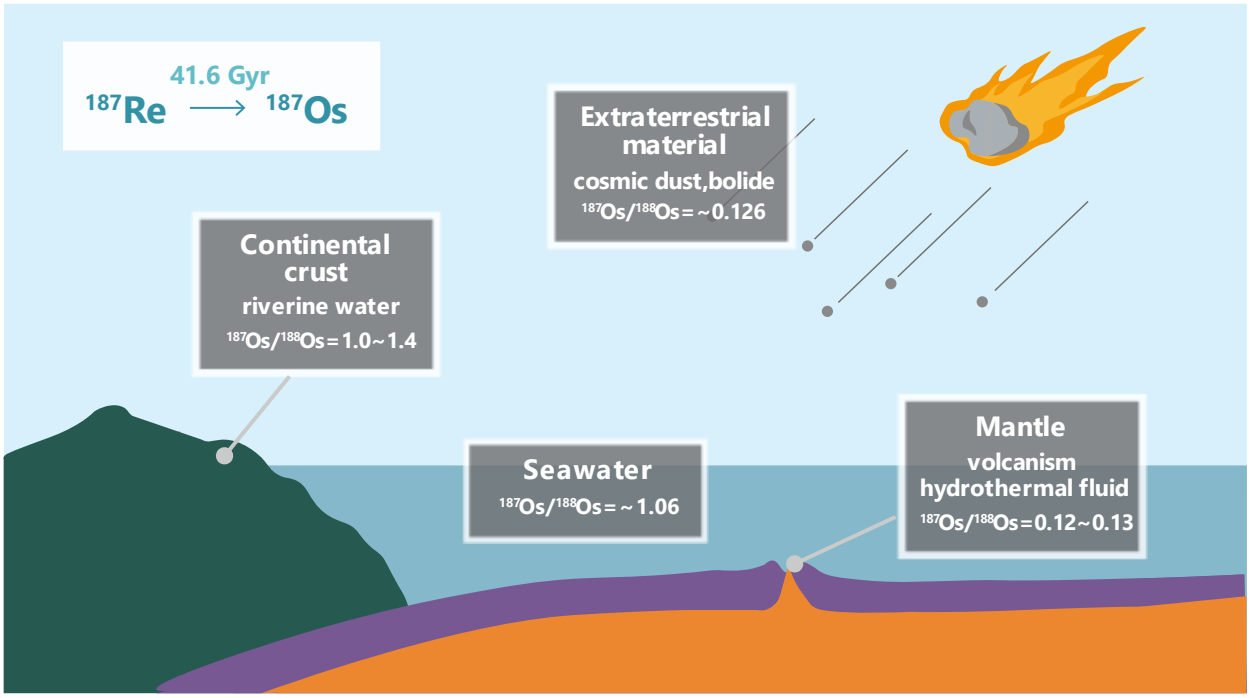


Figure S1B. The marine Osmium isotope system: Data are from Peucker-Ehrenbrink & Ravizza (2000).

## 2. Kawaruppu section

From a small tributary of the Kawaruppu River in the Kawaruppu section, we collected 22 samples from a 200-meter-thick stratigraphic section here, referred to as the "KW section," which were taken for low-resolution analyses across the entire section. The KW section primarily consists of homogenous dark gray mudstone interspersed with frequent calcareous nodules and intercalated with silicic tuff layers. From 171 to 178 m interval sediment is composed of sandy siltstone.

The KRP section, a ~10-meter interval within the KW section, 36 samples were taken for detailed analyses. Eight samples (KWR4) were additionally taken at every ~10 cm interval in the KRP section, for further high-resolution analyses (Figure S2, right). Although classified as mudstone and sandy siltstone, the two lithologies are very similar in appearance, and their grain size difference is barely discernible without magnification (Figure S2, left).

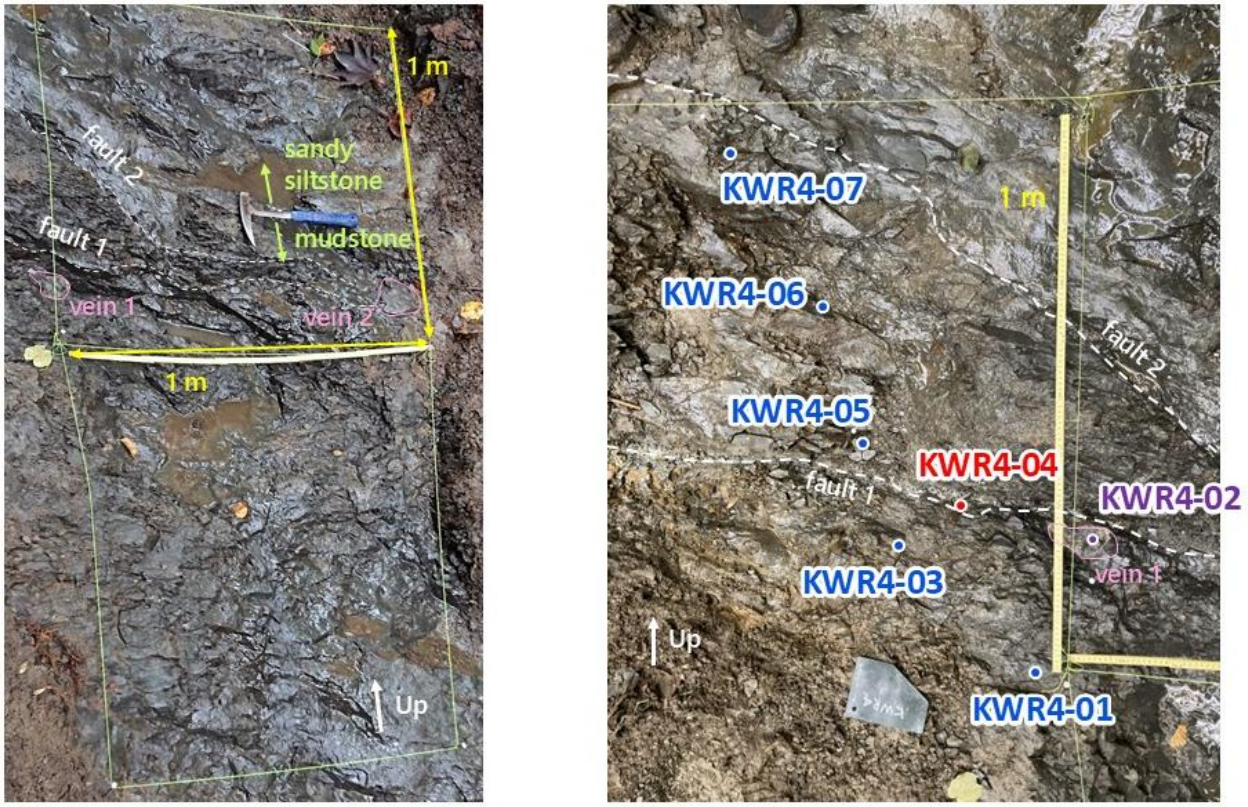


Figure S2. Photo of the area shown in the sketch in Figure 2C (left). Photo of KWR4 sampling point (right).

## 3. Mokawaruppu section

The K-Pg boundary in the Mokawaruppu section was previously presumed to represent complete succession based on paleontological evidence and the presence of a thin clay layer (K-T boundary claystone) (Saito et al., 1986). This boundary clay has long been regarded as the only K-Pg clay layer reported in the northwestern Pacific (e.g., James et al., 2023). However, this clay layer does not exhibit any Ir anomaly (Saito et al., 1986), and no measurements of other PGE concentrations or $^{187}Os/^{188}Os$ ratio have been conducted. In this study, we conducted field surveys in the section and measured PGE concentrations and $^{187}Os/^{188}Os$ ratio of the boundary clay layer (named "MK") to compare with data in the Kawaruppu section (Figure S3A).

Our reinvestigation confirmed that the strata above and below the boundary clay layer (MK) consist of brecciated mudstone (Figure S3C). Their dip and strike orientations differ significantly from those of the surrounding outcrops (Figure S3B).

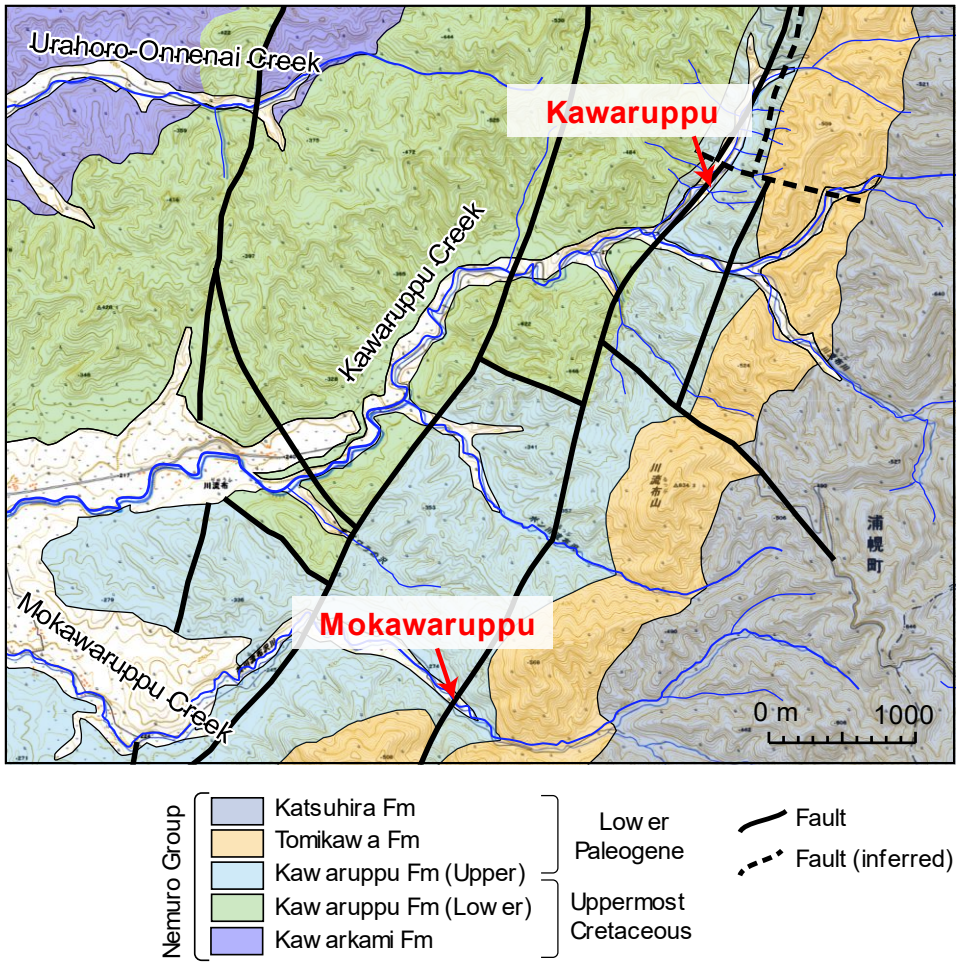


Figure S3A. Location of the Mokawaruppu and Kawaruppu section.

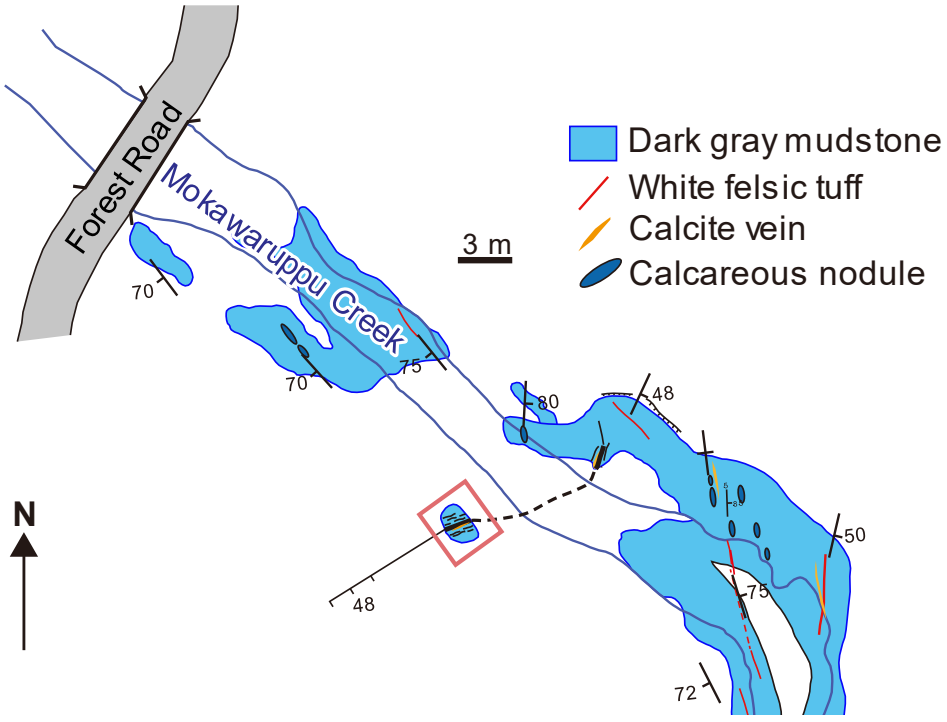


Figure S3B. Route map of Mokawaruppu section. Red square indicates the outcrop including "K-Pg boundary clay layer".

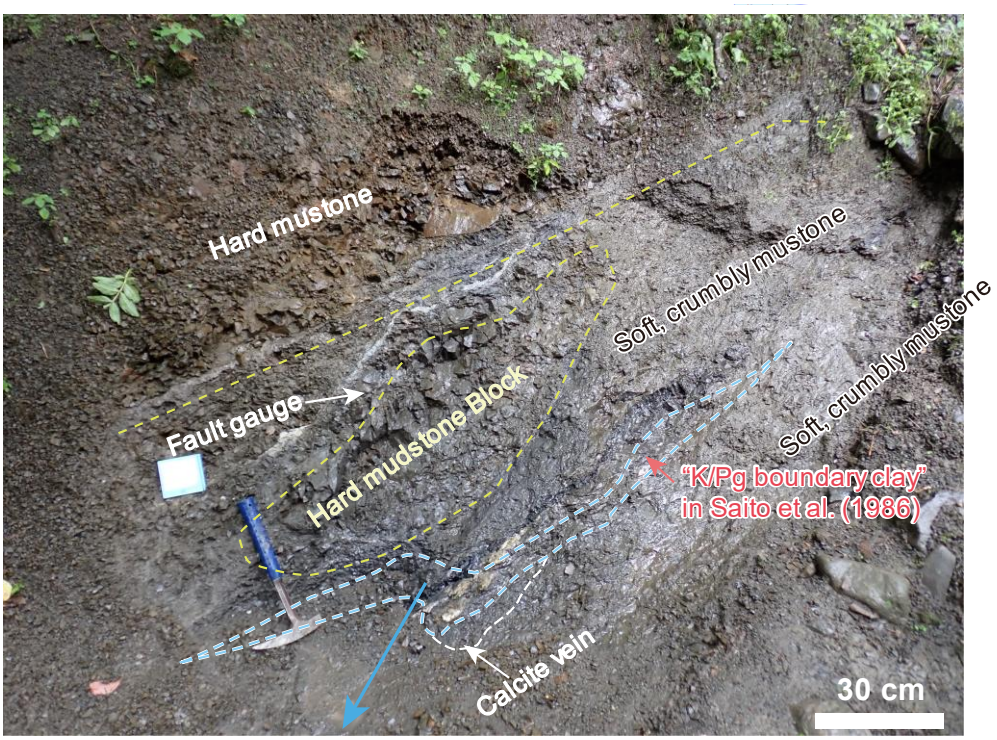


Figure S3C. Photo of "K-Pg boundary clay layer"

## 4. How to measure PGE concentrations and $^{187}Os/^{188}Os$ ratio

We measured Os concentrations and $^{187}Os/^{188}Os$ ratio using negative thermal ionization mass spectrometry (N-TIMS; TRITON, Thermo Fisher Scientific) at JAMSTEC and Re, Ru, Pd, Ir, Pt concentrations using inductively coupled plasma quadrupole mass spectrometer (ICP-QMS; iCAP Q, ThermoFisher Scientific) at JAMSTEC. We used digestion method of Ishikawa et al. (2014) and references therein.

Approximately 0.5 g of powdered samples were weighted, and appropriate amounts of mixed PGE and Re spikes ($^{185}Re$, $^{190}Os$, $^{99}Ru$, $^{105}Pd$, $^{191}Ir$, $^{196}Pt$) were added to a quartz tube. After adding 4 mL of inverse aqua regia, each tube was sealed and heated at 240℃ for 48 hours to achieve sample-spike equilibrium. Os was then separated by solvent extraction into $CCl_4$ and subsequently back-extracted into HBr. To further purify Os, we employed the microdistillation technique described by Nakanishi et al. (2019). The purified Os was loaded onto a platinum filament (Alfa Pt wire), and $Ba(OH)_2$ solution was used as an activator for ionization of Os during measurement. Finally, we analyzed purified Os by N-TIMS. We separated Re, Ru, Pd, Ir and Pt from the inverse aqua regia from which Os was removed by the $CCl_4$ extraction. It was done in three steps: (1) anion exchange chromatography using AG1-X8 resin; (2) solvent extraction using N-benzoyl-N-phenylhydroxylamine (BPHA) and (3) cation exchange chromatography using AG50W-X8 resin. These elements were analyzed by ICP-QMS. All data were corrected for procedural blanks, with average blank values of 0.76 pg for Os and 4.78 pg for Re.

Due to in-situ decay of $^{187}Re$ (decay constant of $1.666 \times 10^{-11}$ $year^{-1}$, Smoliar et al., 1996) producing $^{187}Os$, it was necessary to calculate the initial $^{187}Os/^{188}Os$ ($^{187}Os/^{188}Os_i$) from the measured $^{187}Os/^{188}Os$ value. In this study, the depositional age of all samples was calculated as 66 Ma. If KW and KRP section were assumed to represent the entire C29R chron and corrected accordingly, the resulting difference in $^{187}Os/^{188}Os$ value compared to assuming a uniform age of 66 Ma would be mostly within 0.03%. Therefore, assuming a uniform age of 66 Ma for all samples does not significantly affect the results.

## 5. Measurement results of PGE concentrations and $^{187}Os/^{188}Os$ ratio of KRP samples and MK

The Re and PGE concentrations in KWR4-02 (vein) and KWR4-tuff samples are either significantly lower or roughly comparable to those of other samples from the KRP section. The $^{187}Os/^{188}Os$ ratio in KWR4-tuff is relatively high, with a value of 0.6. These results suggest that the PGE composition of this section was not influenced by local features such as veins or tuffs.

The Re and PGE concentrations in MK are also comparable to those in the KRP section, and notably, the Re concentration and $^{187}Os/^{188}Os$ ratio are nearly identical to those found in the Danian sediment of the KRP section. These lines of evidence suggest that the K-Pg impact ejecta layer is not preserved in the Mokawaruppu section.

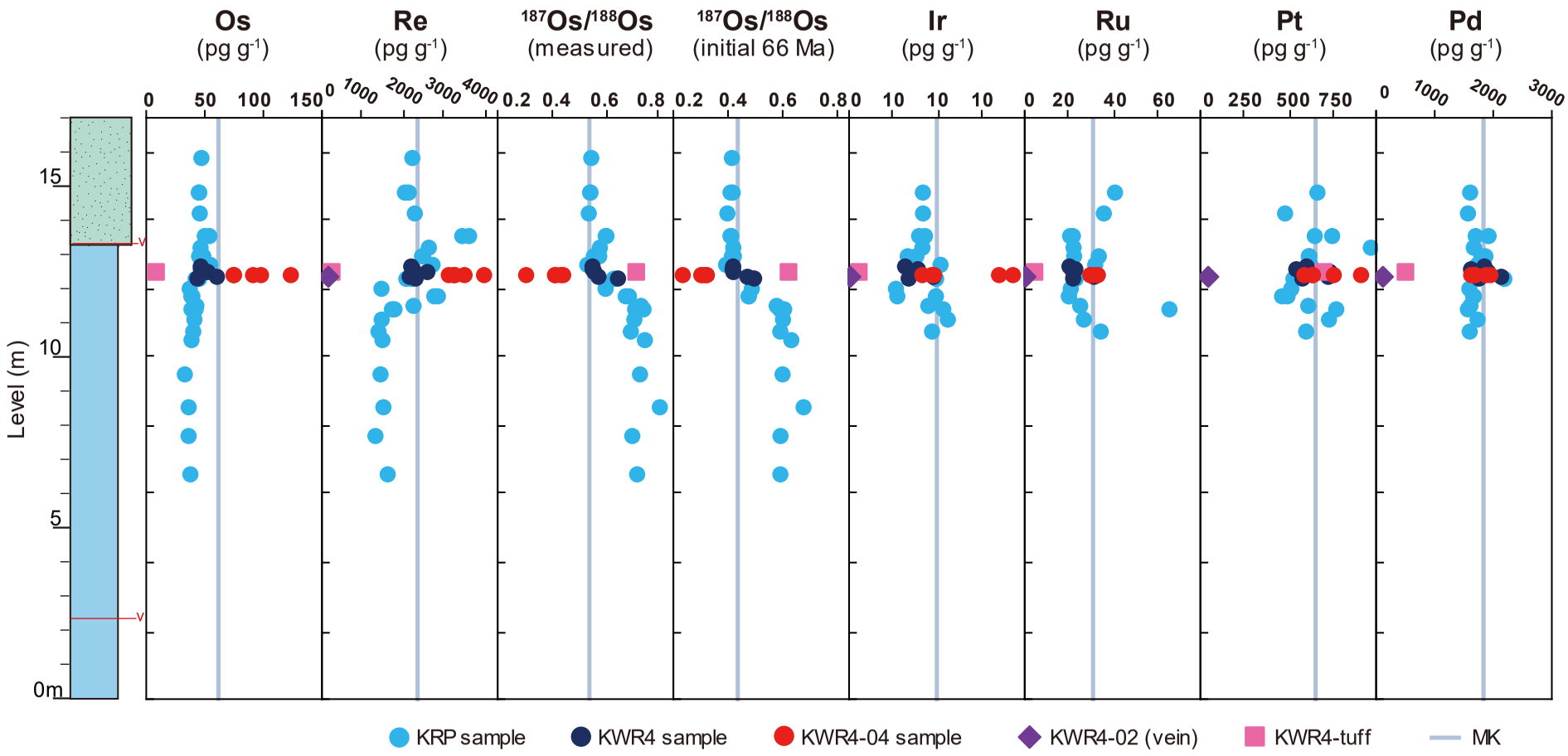


Figure S5. Re and PGE concentrations and $^{187}Os/^{188}Os$ ratio of KRP section and MK

## 6. Sedimentation rate in KW section

We estimated the sedimentation rate in the KW section using 1) the stratigraphic level of the K-Pg boundary (173.1 m) identified based on our $^{187}Os/^{188}Os_i$ and PGE data, 2) zircon U-Pb ages for tuff layers (178 m and 188 m) and 3) paleomagnetic reversals. By assuming that the base of the KW section (0 m) corresponds to the C29R/C30N boundary (63.380 Ma) and the top of the KW section (255 m) corresponds to the C29N/C29R boundary (65.700 Ma), a minimum sedimentation rate can be estimated (Figure S6).

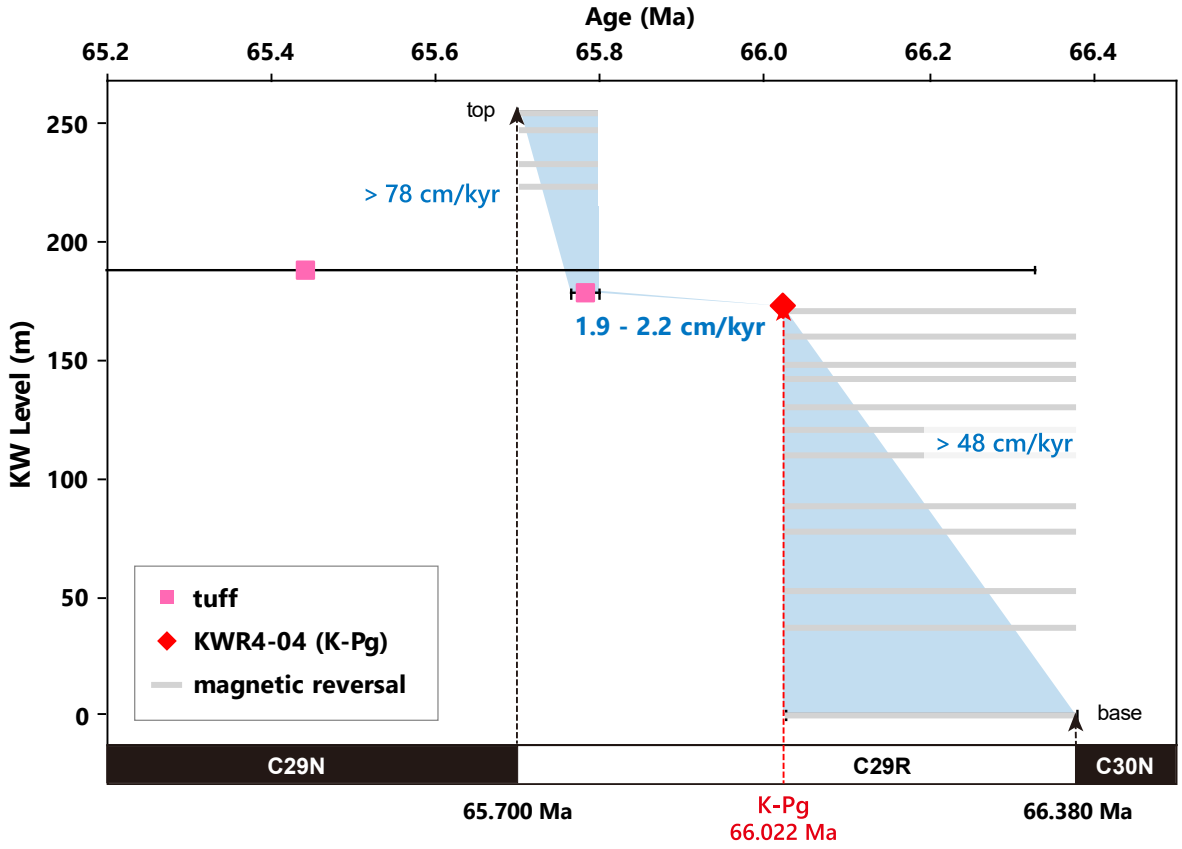


Figure S8. Age-Depth profile for the KW section. The numerical ages with error bars were obtained for the two layers of tuff (zircon U-Pb age, shown in pink square) and the K-Pg boundary (KWR04-04, shown in red diamond, age and uncertainties of K-Pg boundary were provided by Westerhold et al., 2025). Gray horizontal lines indicate the possible range based on paleomagnetic data. Light blue area indicates all possible age ranges for the given stratigraphic interval.

## 7. Calculation of Os/Ir and $^{187}Os/^{188}Os$ ratio recovery

We performed a simple model calculation of the recovery of the Os/Ir ratio after impact, referring to Ravizza & VonderHaar (2012) (Supplementary 3) to estimate the missing interval at the K-Pg boundary. First, the concentration of each element changes over time as follows:

$$\frac{dC}{dt} = \frac{C_{ss} - C}{\tau}$$

where C is the concentration of Os or Ir, t is time, and τ is the marine residence time of Os or Ir. The subscript "ss" denotes steady state. Solving this equation, we obtain:

$$C(t) = (C_{ss} - C_0) * e^{-t/\tau} \qquad (1)$$

here, t = 0 is the time of the K-Pg impact, and C0 is the Os or Ir concentrations of sediment when impact-derived Os and Ir were supplied (i.e. concentration at the K-Pg just boundary). The Os/Ir ratio can be written as follows:

$$\left(\frac{Os}{Ir}\right)_{sediment} = \frac{\{C_{ss(Os)} - (C_{ss(Os)} - C_{0(Os)}) * e^{-t/\tau(Os)}\}}{\{C_{ss(Ir)} - (C_{ss(Ir)} - C_{0(Ir)}) * e^{-t/\tau(Ir)}\}} \qquad (2)$$

We applied the data from KRP section to this equation and simulated it (Figure S2B), where Css(Os) and Css(Ir) were set to 97 pg $g^{-1}$ and 16 pg $g^{-1}$, respectively, the average of the stable values in Danian. The Os concentration of KWR4-04 is approximately 250 pg $g^{-1}$, indicating that C0(Os) must be at least 250 ppt. Three scenarios were considered for C0(Os): 250, 300, and 350 pg $g^{-1}$. According to Lee et al. (2003), the Os/Ir ratio at the K-Pg boundary in hemipelagic regions (Stevns Klint in Denmark and Caravaca in Spain) ranges from 0.633 to 0.808. Therefore, C0(Ir) was set such that C0(Os)/C0(Ir) = 0.7.

The modern residence time of Os and Ir in the ocean is estimated to be 10–40 kyr and 2–20 kyr, respectively (Levasseur et al., 1999; Oxburgh et al., 1998; Anbar et al., 1996). To cover a range of plausible scenarios, the shortest residence time combination (τ(Os) = 10 kyr, τ(Ir) = 2 kyr) and the longest residence time combination (τ(Os) = 40 kyr, τ(Ir) = 6 kyr) were considered. A total of six scenarios were established by combining the three C0(Os) values with the two residence time settings to simulate the variation in the Os/Ir ratio following the K-Pg impact.

Calculation of $^{187}Os/^{188}Os$ ratio

Replacing Css(Os), Css(Ir), C0(Os) and C0(Ir) in (2) as Css($^{188}$Os), Css($^{188}$Os), C0($^{187}$Os) and C0($^{188}$Os), respectively, gives the following formula:

$$R_{(t)} = (R_{ss} - (R_{ss} - R_0 * E) * e^{\left(-\frac{t}{\tau}\right)})/(1 - (1 - E) * e^{\left(-\frac{t}{\tau}\right)}) \qquad (3)$$

where $R_{ss} = C_{ss(^{187}Os)}/C_{ss(^{188}Os)}$, $R_0 = C_{0(^{187}Os)}/C_{0(^{188}Os)}$ and $E = C_{0(^{188}Os)}/C_{ss(^{188}Os)}$.

The seawater Os isotope ratio immediately after the meteorite impact can be expressed as follows:

$$R_0 = f_{ss} * R_{ss} + f_m * R_m$$

where fss, fm and Rm are the fraction of Os in seawater derived from the original seawater source after the impact, the fraction of Os in seawater derived from the meteorite after the impact and the $^{187}Os/^{188}Os$ ratio of the meteorite, respectively. Since $f_{ss} + f_m = 1$, the following expression for fm is obtained:

$$f_m = (R_{ss} - R_0)/(R_{ss} - R_m) \qquad (4)$$

The seawater $^{188}Os$ concentration immediately after the impact can be expressed as follows:

$$C_{0(^{188}Os)} = C_{ss(^{188}Os)} + f_m * C_{0(^{188}Os)}$$

Therefore,

$$E = C_{0(^{188}Os)}/C_{ss(^{188}Os)} = 1/(1 - f_m) \qquad (5)$$

Combining (4) and (5) to eliminate f_m gives

$$E = (R_{ss} - R_m)/(R_o - R_m) \qquad (6)$$

Here, Rss and Rm were fixed as the average $^{187}Os/^{188}Os_i$ ratio in the Danian of the KRP section (0.414) and the average value for chondrites (0.127) reported by Horan et al. (2003), respectively. The Ro value was set to three patterns: 0.157 (the K-Pg boundary at DSDP 577; Paquey et al., 2008), 0.200 (the approximate global average of the K-Pg boundary), and 0.251 (the K-Pg boundary at Gubbio; Robinson et al., 2009). A total of six scenarios were established by combining the three Ro values with the two residence time settings to simulate the variation in the $^{187}Os/^{188}Os_i$ ratio following the K-Pg impact.

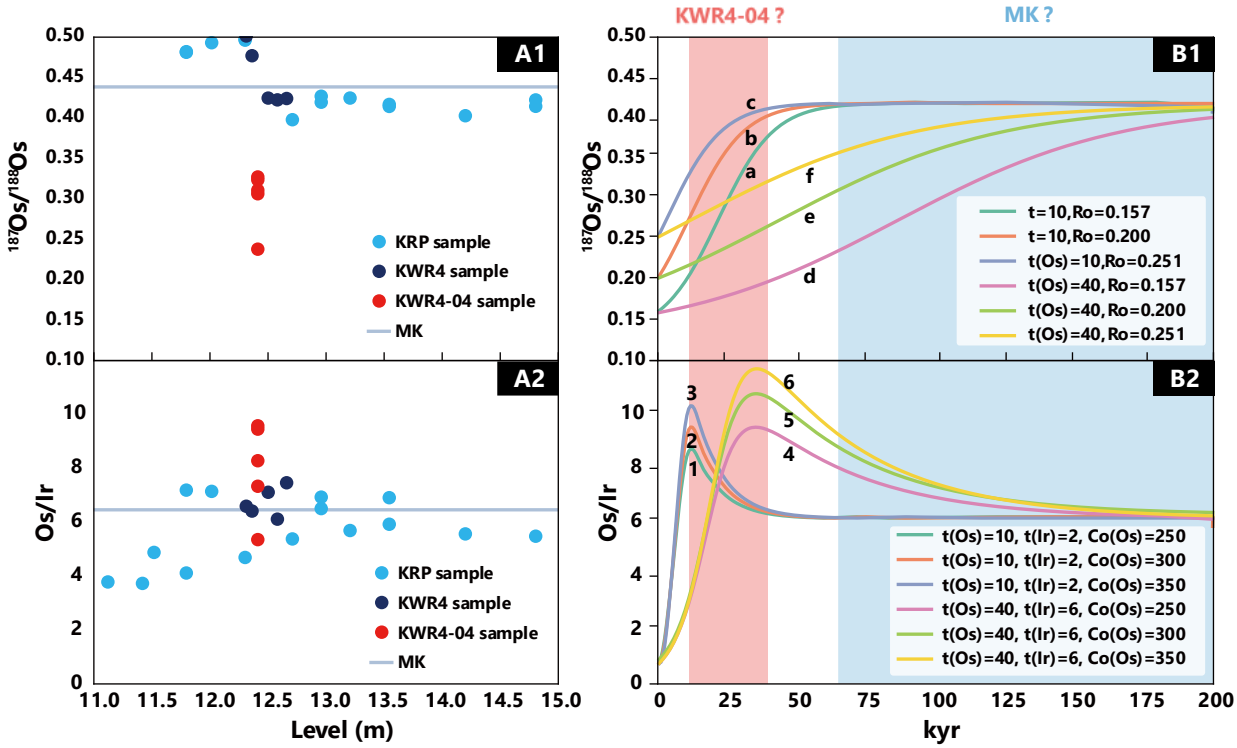


Figure S7 (A1) $^{187}Os/^{188}Os$ ratio of the KRP section. (A2) Os/Ir ration of the KRP section. (B1) Calculated recovery of the $^{187}Os/^{188}Os$ ratio of the KRP section following the K-Pg impact. (B2) Calculated recovery of the Os/Ir ratio of the KRP section following the K-Pg impact.

## 8. Measurement results of major elements

We also measured major element composition of KWR4 samples using a RIGAKU ZSX Primus Ⅱ X-ray fluorescence (XRF) spectrometer at Atmosphere and Ocean Research Institute (AORI), the University of Tokyo (Kashiwa) to confirm that the composition of the platinum group elements is not due to changes in the composition of the base rock. All work was conducted at AORI. The sample powders used for this measurement were the same as those for PGE measurement.

The LOI (loss of ignition) values are in the range of ~3.6-4.2 wt%, with small amounts of volatile components. Only KWR4-04 and 04" have slightly higher LOI than the other samples (4.0381 and 4.1522, respectively). The major element compositions were almost similar for all samples (Figure S8).

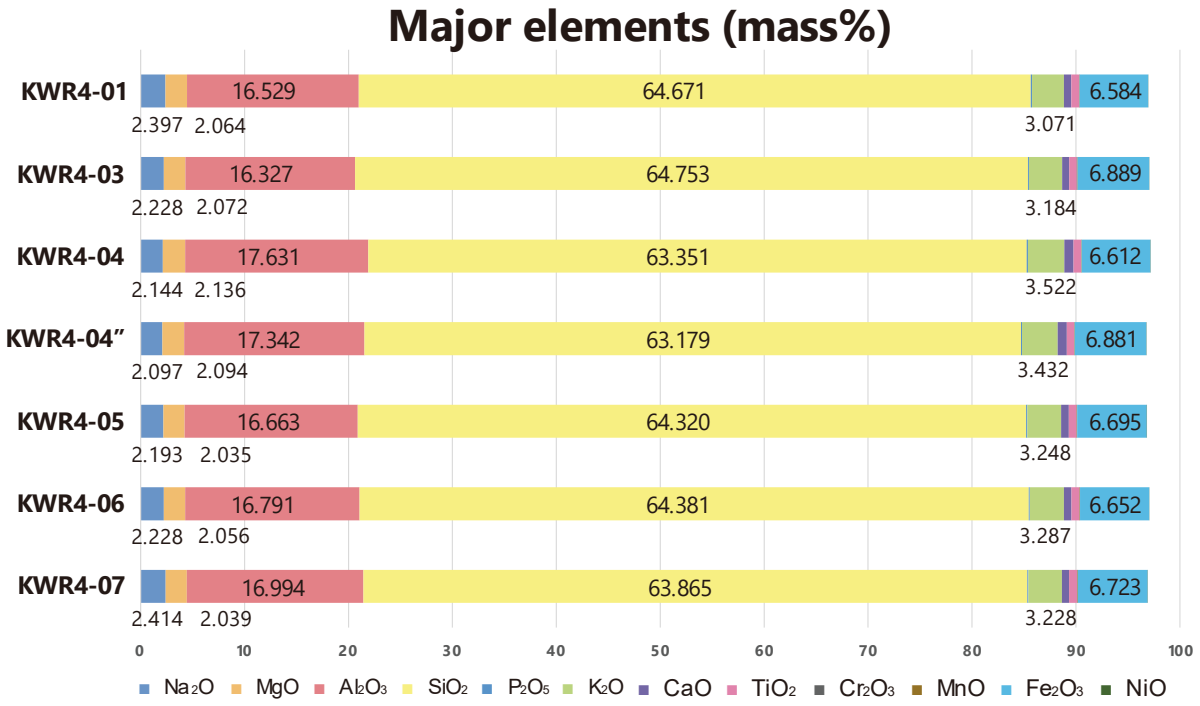


Figure S8. Major element results of KWR4 samples

## 9. Thin section of KWR4-04 and 05 samples

We prepared thin sections only from the KWR4-04 and KWR4-05 samples. Pyrite, which is commonly found in reducing environments, along with wood fragments and broken mineral grains, was observed (Figure S9A, B). However, no physical evidence of a meteorite impact, such as spherules or shocked quartz, was identified.

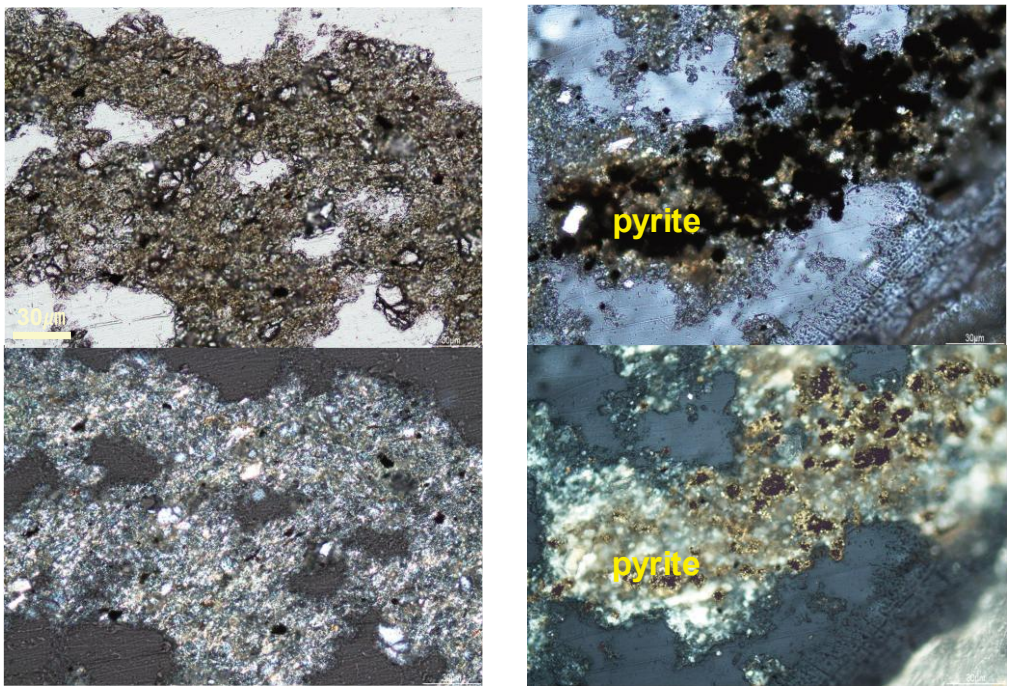


Figure S9A. Thin section of KWR4-04 sample

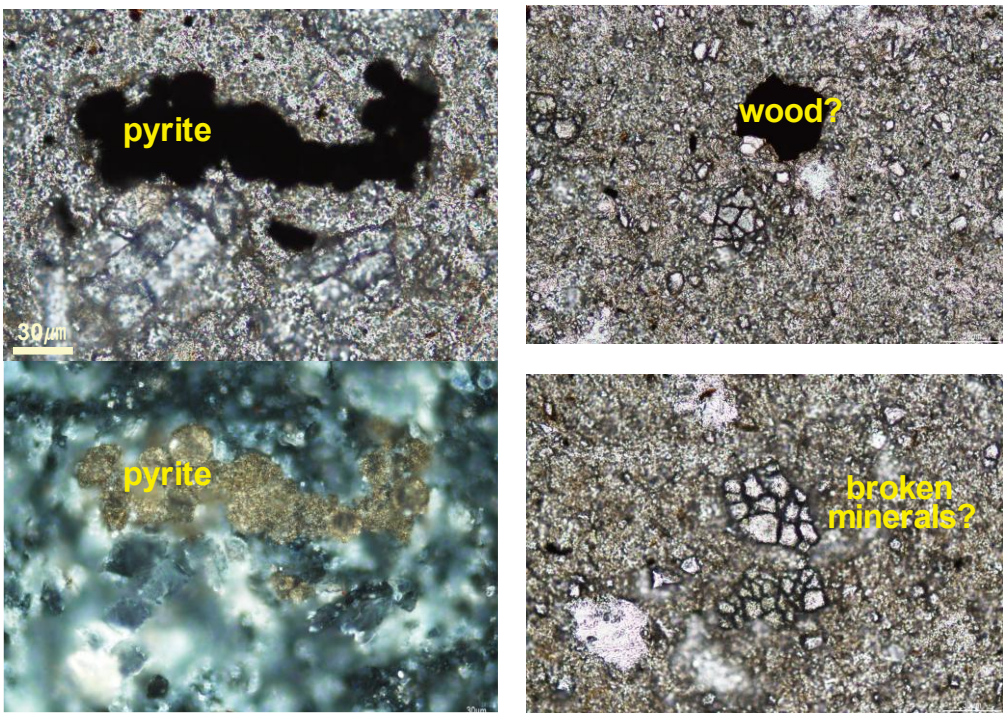


Figure S9B. Thin section of KWR4-05 sample

## 10. Biomarker in KRP section

Hayashi et al. (2023) measured pristane/phytane (Pr/Ph ratio), homophopane index (HHI), and C27/(C27+C29) sterane ratio measurements, which indicate an oxidizing environment (Figure S10). The C27/(C27+C29) sterane ratios indicate the land/sea contribution of organic matter: C27 steranes are from marine eukaryotic algae and C29R steranes are from terrestrial plants. The high Pr/Ph ratio can be attributed to the high contribution of terrestrial plants. From the above it can be concluded that the sedimentary field itself was to some extent reducing and had a high influx of organic matter from terrestrial sources.

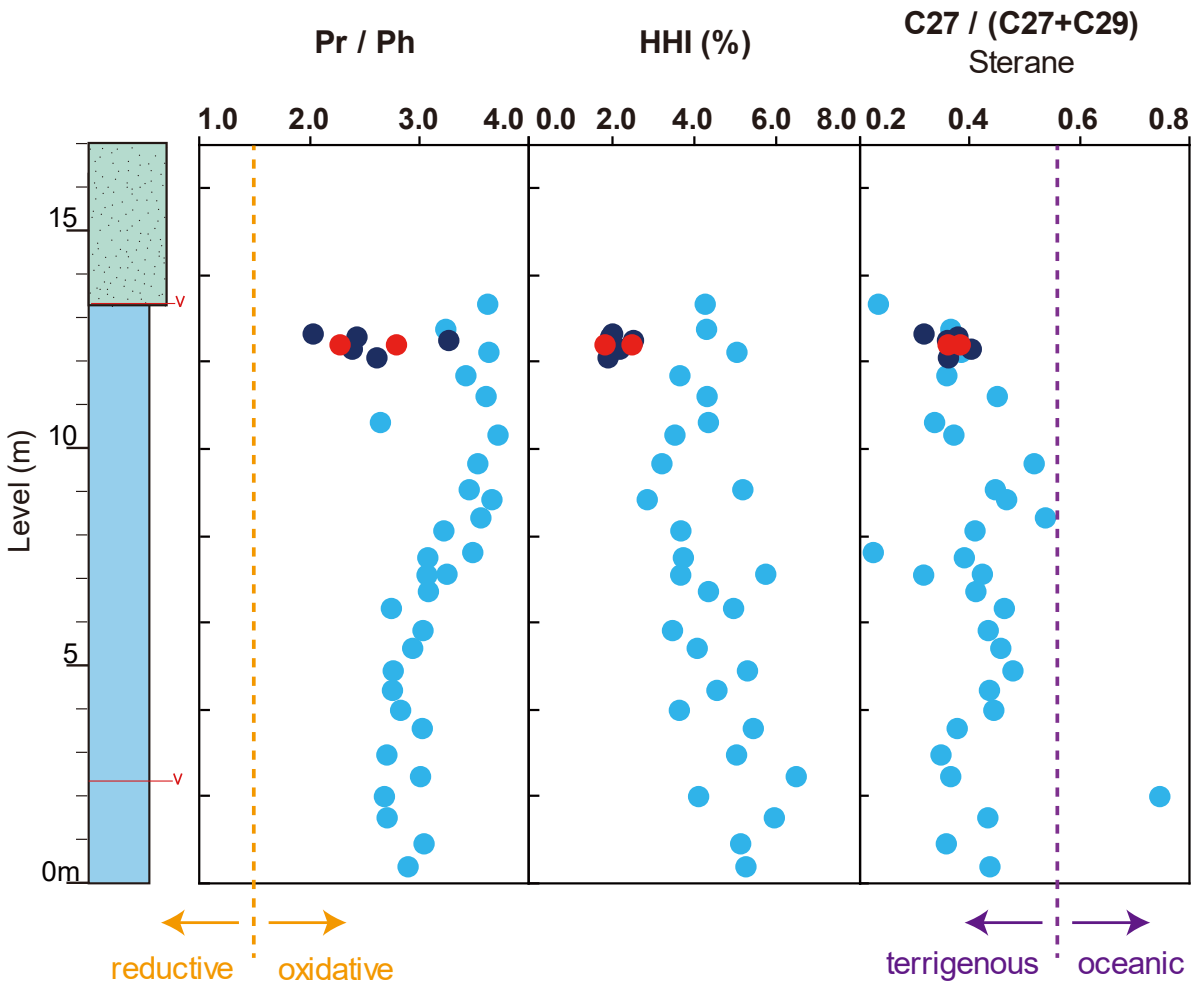


Figure S10. Pr/Ph ratio, the HHI indicator and C27/(C27+C29) sterane of the KRP section

## 11. Future works

We conducted additional sampling in the KRP section last August. By measuring the PGE concentration and $^{187}Os/^{188}Os$ ratio of these samples, we will obtain extremely high-resolution data.

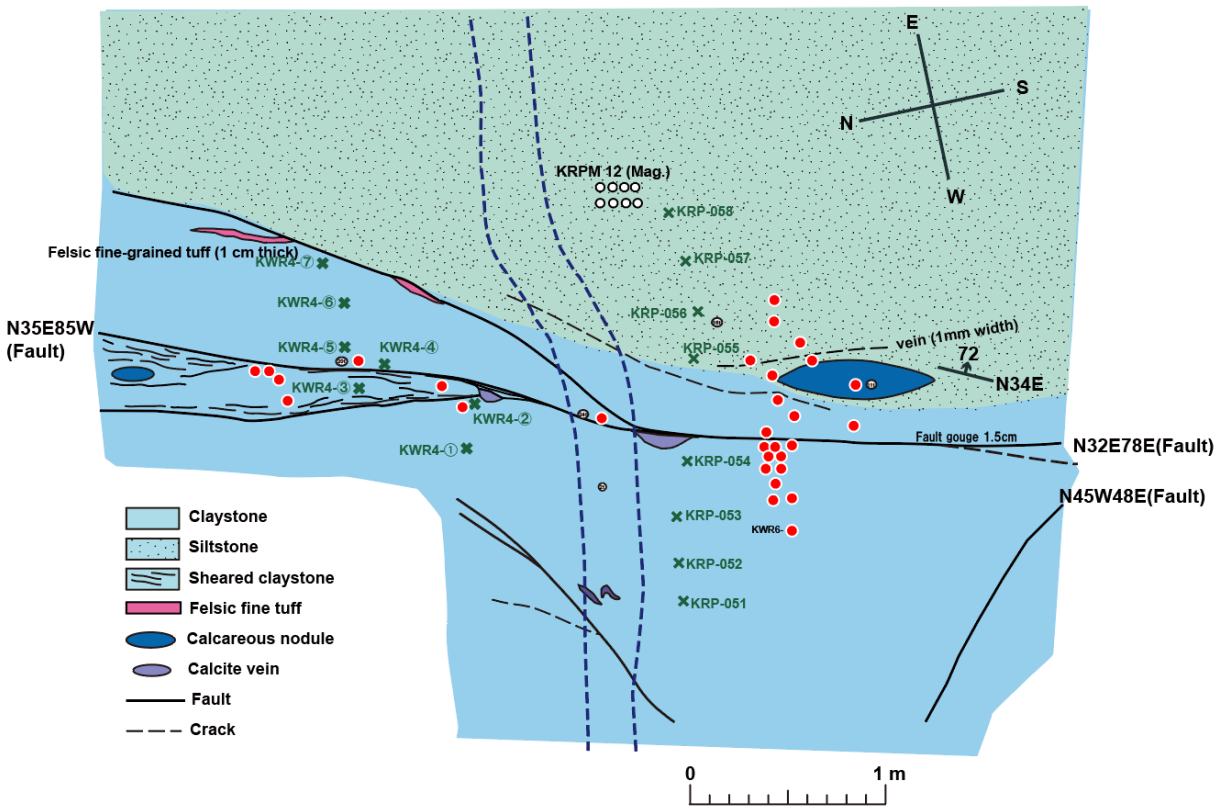


Figure S11. Outcrop sketch of the area with geochemical evidence of the Chicxulub impact. Red dots indicate additional sampling points.

## References


Anbar, A. D., Wasserburg, G. J., Papanastassiou, D. A., and Andersson, P. S., 1996, Iridium in natural waters: Science, v. 273(5281), p. 1524-1528, https://doi.org/10.1126/science.273.5281.1524

Hayashi, K., Ikeda, M. A., Sawada, K., Hayashi, K., Takashima, R., Nishi, H., Kuroda, J., and Ota, H., Paleoenvironmental reconstruction by biomarker analyses of sedimentary rocks deposited across the Cretaceous/Paleogene boundary in the Nemuro Group, Hokkaido, Japan. Presented at the 130th Annual Meeting of the Geological Society of Japan. Kyoto. Japan, September 17-19, 2-23.

Horan, M. F., Walker, R. J., Morgan, J. W., Grossman, J. N., and Rubin, A. E., 2003, Highly siderophile elements in chondrites: Chemical Geology, v. 196(1-4), p. 27-42, https://doi.org/10.1016/S0009-2541(02)00405-9

Ishikawa, A., Senda, R., Suzuki, K., Dale, C. W., and Meisel, T., 2014, Re-evaluating digestion methods for highly siderophile element and 187Os isotope analysis: Evidence from geological reference materials: Chemical Geology, v. 384, p. 27-46, https://doi.org/10.1016/j.chemgeo.2014.06.013

James, S., Chandran, S. R., Aswathi, J., Padmakumar, D., and Sajinkumar, K. S., 2023, Geologic, geomorphic, tectonic, and paleoclimatic controls on the distribution and preservation of Chicxulub distal ejecta: A global perspective: *Earth-Science Reviews*, v. *244*, no. 104545, https://doi.org/10.1016/j.earscirev.2023.104545

Lee, C. T. A., Wasserburg, G. J., and Kyte, F. T., 2003, Platinum-group elements (PGE) and rhenium in marine sediments across the Cretaceous–Tertiary boundary: constraints on Re-PGE transport in the marine environment: Geochimica et Cosmochimica Acta, v. 67, no. 4, p. 655-670, https://doi.org/10.1016/S0016-7037(02)01135-3

Levasseur, S., Birck, J. L., and Allegre, C. J., 1999, The osmium riverine flux and the oceanic mass balance of osmium: Earth and Planetary Science Letters, v. 174(1-2), p. 7-23, https://doi.org/10.1016/S0012-821X(99)00259-9

Nakanishi, N., Yokoyama, T., and Ishikawa, A., 2019, Refinement of the Micro-Distillation Technique for Isotopic Analysis of Geological Samples with pg-Level Osmium Contents: Geostandards and Geoanalytical Research, v. 43(2), p. 231-243, https://doi.org/10.1111/ggr.12262

Oxburgh, R., 1998, Variations in the osmium isotope composition of sea water over the past 200,000 years: Earth and Planetary Science Letters, v. 159(3-4), p. 183-191, https://doi.org/10.1016/S0012-821X(98)00057-0

Paquay, F. S., Ravizza, G. E., Dalai, T. K., and Peucker-Ehrenbrink, B., 2008, Determining chondritic impactor size from the marine osmium isotope record: Science, v. 320, p. 214-218, doi:10.1126/science.1152860

Peucker-Ehrenbrink, B. and Ravizza, G., 2000, The marine osmium isotope record: Terra Nova, v. 12.5, p. 205-219, doi:10.1046/j.1365-3121.2000.00295.x

Ravizza, G. and VonderHaar, D., 2012, A geological clock in earliest Paleogene pelagic carbonates based on the impact-induced Os isotope excursion at the Cretaceous-Paleogene boundary: Paleoceanography, v. 27, PA3219, https://doi.org/10.1029/2012PA002301

Robinson, N., Ravizza, G., Coccioni, R., Peucker-Ehrenbrink, B., and Norris, R., 2009, A high-resolution marine $^{187}Os/^{188}Os$ record for the late Maastrichtian: Distinguishing the chemical fingerprints of Deccan volcanism and the KP impact event: Earth and Planetary Science Letters, v. 281, p. 159-168, https://doi.org/10.1016/j.epsl.2009.02.019

Saito, T., Yamanoi, T., and Kaiho, K., 1986, End-Cretaceous devastation of terrestrial flora in the boreal Far East: Nature, v. 323, p. 253-255.

Sharma, M., 2019, Platinum Group Elements and Their Isotopes in the Ocean: Encyclopedia of Ocean Sciences (Third Edition), v .1, p. 174-180, https://doi.org/10.1016/B978-0-12-409548-9.11556-8

Smoliar, M. I., Walker, R. J., and Morgan, J. W., 1996, Re-Os ages of group IIA, IIIA, IVA, and IVB iron meteorites: Science, v. 271(5252), p. 1099-1102, https://doi.org/10.1126/science.271.5252.1099

Westerhold, T., Dallanave, E., Penman, D., Schoene, B., Röhl, U., Gussone, N., and Kuroda, J., 2025, Earth orbital rhythms links timing of Deccan trap volcanism phases and global climate change: Science Advances, v. 11, no. 10, https://doi.org/10.1126/sciadv.adr8584